Modeling Gas Effects in a Bubbling Fluidized Bed Reactor for Biomass Pyrolysis

Gavin M. Wiggins, Oluwafemi A. Oyedeji

July 27, 2020

Contents

Abstract

Fast pyrolysis of biomass in a fluidized bed reactor is typically conducted in a nitrogen gas environment. Recycling product gas can improve the economics of operating such a system by reducing reliance on pure process streams.

1 Introduction

Fast pyrolysis is a versatile method for thermochemical conversion of solid biomass into liquid bio-oil which can be used for bio-fuel and high-value chemical production. Bio-oil is commonly generated in bubbling fluidized bed and circulating fluidized bed reactor systems in which biomass particles rapidly devolatilize in the absence of oxygen into mixtures of light gases, condensable bio-oil vapors, and solid char [4, 5, 16]. Since biomass pyrolysis normally occurs in a non-oxidizing environment, the fluidization gas (carrier gas) is often pure nitrogen [16]. To maximize bio-oil yields, the reactor typically operates at temperatures near 500°C and must maintain particle residence times up to 10 seconds and gas residence times less than 2 seconds [5]. Deviations from these conditions can result in significant production and quality penalties, therefore optimal reactor design and control become crucial to achieving commercially viable bio-oil production.

To improve the economic possibilities of biomass fast pyrolysis systems, char can be burned for process heat while recycled pyrolysis gas can assist with fluidization [4, 14]. The major generated components of pyrolysis gas are CO, CO_2, CH_4, H_2, and other light hydrocarbons [1, 23]. Several experiments investigated the effects of these gases on reactor conditions and pyrolysis yields [14, 17, 23] but modeling the effects of the different gases was not discussed.

There are several models available that investigate the hydrodynamics and conversion of biomass at fast pyrolysis conditions in fluidized bed reactors [20, 15]. As is typical for biomass pyrolysis, these models assume the fluidization gas is pure nitrogen. The authors are not aware of any published models in the biomass pyrolysis literature that account for the effects of fluidization or carrier gas other than nitrogen.

This paper uses engineering correlations, reduced-order modeling techniques, and CFD simulations to investigate the effects of gas mixtures in a fluidized bed biomass pyrolysis reactor. The scope of this study is to evaluate different gas mixtures and there effects on the hydrodynamics and biomass conversion in fluidized bed reactors operating at fast pyrolysis conditions.

2 Experimental apparatus

The NREL 2FBR reactor system thermochemically converts biomass feedstock at fast pyrolysis conditions. The system is comprised of two bubbling fluidized bed (BFB) reactors where the first reactor is for biomass fast pyrolysis and the second reactor is for vapor phase upgrading. Modeling activities discussed in this paper refer to the BFB pyrolysis reactor.

An overview of the NREL 2FBR system is shown in Figure 1, components of the pyrolysis reactor are detailed in Figure 2, while dimensions and typical operating conditions of the pyrolysis unit are given in Figure 3. Sand is used as the dominant heat transfer medium in the pyrolyzer. Biomass particles are fed to the reactor via a screw auger and nitrogen is used as the fluidization/carrier

gas. More information about the NREL 2FBR biomass pyrolysis system is available elsewhere [11, 21].

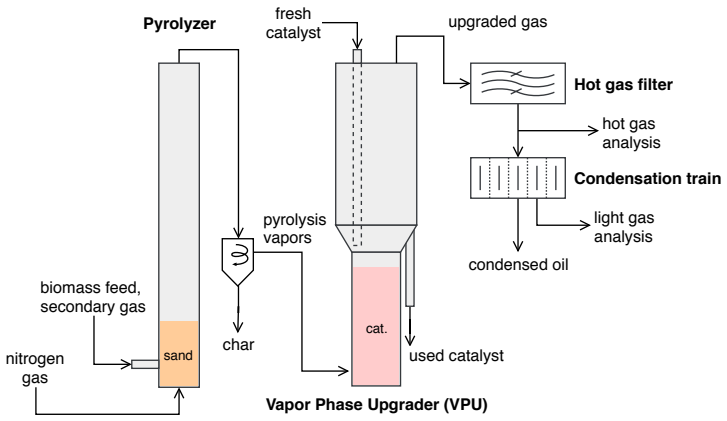

Figure 1: Overview of the NREL 2FBR system. Biomass fast pyrolysis occurs in the pyrolyzer (left) and gaseous products are catalytically upgraded in the vapor phase upgrader (right).

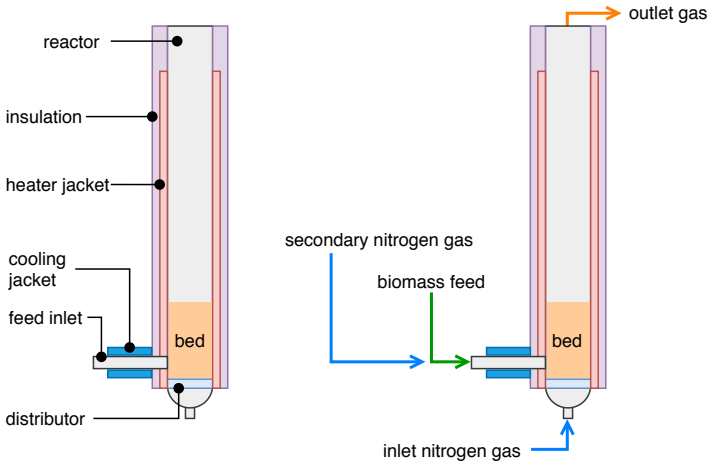

Figure 2: Components of the BFB biomass pyrolysis reactor referred to as the "pyrolyzer" in the NREL 2FBR system.

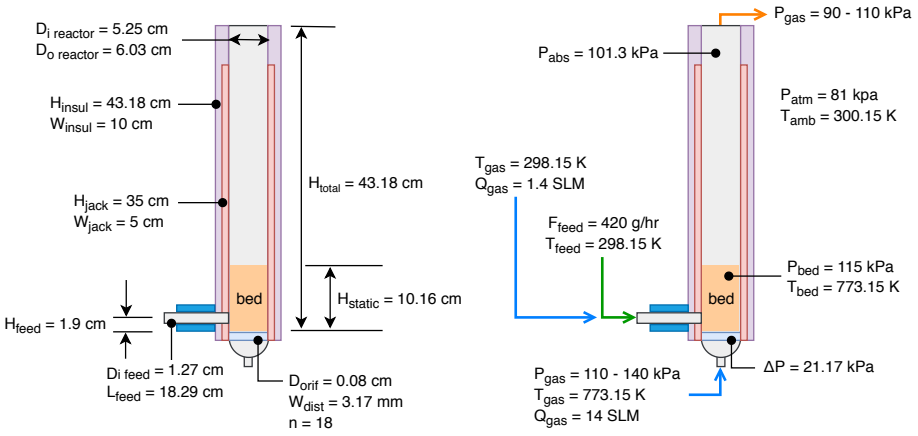

Figure 3: Dimensions and typical fast pyrolysis operating conditions for the BFB biomass pyrolysis reactor in the NREL 2FBR system.

3 Modeling approach

Engineering correlations, reduced-order models, and CFD modeling techniques were used to investigate the effects of recycled gas on the operation of a fluidized-bed biomass pyrolysis reactor. The following sections discuss approaches implemented in this work for calculating gas properties and the associated effects on fluidization conditions and pyrolysis yields.

3.1 Gas properties

Density of the gas is calculated from the ideal gas law as shown in Equation 1 where ρ_{gas} is density (kg/m^3), P is pressure (Pa), MW is molecular weight (g/mol), R is the gas constant [(m^3 Pa) / (K mol)], and T is temperature (K).

$$\rho_{gas} = \frac{P\,MW}{R\,T} \tag{1}$$

Gas viscosity (μ_{gas} as μP) is determined from Equation 2, thermal conductivity (k_{gas} as W/m K) is estimated from Equation 3, and heat capacity ($C_{p\,gas}$ as J/mol K) is calculated from Equation 4. Temperature of the gas in Kelvin is represented by T while the regression coefficients A, B, C, D, E, F, and G for each gas are obtained from Yaws' Handbook [22].

$$\mu_{gas} = A + B\,T + C\,T^2 + D\,T^3 \tag{2}$$

$$k_{gas} = A + B\,T + C\,T^2 + D\,T^3 \tag{3}$$

$$C_{p\,gas} = A + B\,T + C\,T^2 + D\,T^3 + E\,T^4 + F\,T^5 + G\,T^6 \tag{4}$$

Several methods are available to calculate the viscosity of a gas mixture. Equation 5 calculates the mixture viscosity from the sum of the mole fraction and viscosity product of each gas component in the mixture [9] while Equation 6 accounts for the molecular weight of each gas component [10].

$$\mu_{mix} = \sum(x_i \cdot \mu_i) \tag{5}$$

$$\mu_{mix} = \frac{\sum(\mu_i \cdot x_i \cdot \sqrt{MW_i})}{\sum(x_i \cdot \sqrt{MW_i})} \tag{6}$$

The Prandtl number is a dimensionless number representing the ratio of momentum diffusivity to thermal diffusivity. It is calculated from the equation shown below where C_p is heat capacity (J/kg·K), μ is dynamic gas viscosity (kg/m·s), and k is thermal conductivity (W/m·K).

$$Pr = \frac{C_p\,\mu}{k} \tag{7}$$

3.2 Fluidization correlations

For a bed of particles, the minimum fluidization velocity U_{mf} is the gas velocity at which the drag force of the upward moving gas equals the weight of the particles. Kunii and Levenspiel [12] provide the following equation for calculating minimum fluidization velocity

$$U_{mf} = \frac{Re_{p,mf}\mu}{d_p\rho_g} \tag{8}$$

where μ is gas viscosity (kg/m s), d_p is particle diameter (m), ρ_g is gas density (kg/m^3), and $Re_{p,mf}$ is the particle Reynolds number (-) at minimum fluidization conditions. The Reynolds number is calculated from the Archimedes number (Ar) and two dimensionless constants (a, b) which represent experimental coefficients. Different U_{mf} correlations were evalutaed based on experimental data from Wen and Yu where $(a, b) = (33.7, 0.0408)$, from Richardson where $(a, b) = (25.7, 0.0365)$, and from Grace where $(a, b) = (27.2, 0.0408)$ [12].

$$Re_{p,mf} = \left(a^2 + bAr\right)^{1/2} - a \tag{9}$$

$$Ar = \frac{d_p^3\rho_g(\rho_s - \rho_g)g}{\mu^2} \tag{10}$$

According to Kunii and Levenspiel [12], the constants (a, b) can be derived from the Ergun pressure drop equation based on the constants K_1 and K_2 where ϵ_{mf} is the bed void fraction (-) at minimum fluidization and ϕ is sphericity (-) of the bed particles. For this paper, U_{mf} is estimated based on the Ergun, Grace, Richardson, and Wen and Yu correlations.

$$a = \frac{K_2}{2K_1} \qquad b = \frac{1}{K_1} \tag{11}$$

$$K_1 = \frac{1.75}{\epsilon_{mf}^3 \phi} \qquad K_2 = \frac{150(1-\epsilon_{mf})}{\epsilon_{mf}^3 \phi^2} \tag{12}$$

3.3 Pyrolysis kinetics

A pyrolysis kinetics scheme based on the work of Di Blasi was implemented to predict the conversion of biomass into gas, tar, and char products [2, 3]. Figure 4 gives an overview of the scheme and its reaction mechanisms. Reactions 1–3 represent the primary conversion of biomass while reactions 4–5 are secondary reactions that reduce tar yield at long residence times.

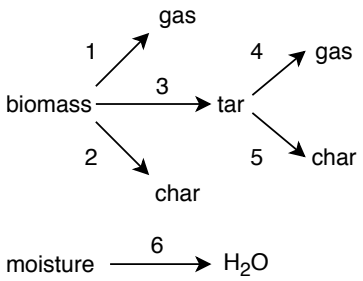

Figure 4: Diagram of the Di Blasi pyrolysis kinetics scheme for conversion of biomass to gas, tar, and char products.

The pyrolysis reactions were modeled as first-order Arrhenius type equations where the reaction rate is given as

$$r_i = C_i \, A_i \, e^{-E_i/RT} \tag{13}$$

where r_i is the rate of reaction i such that C_i is a mass based concentration, A_i is the pre-factor (1/s), E_i is the activation energy (kJ/mol), R is the gas constant, and T is the reaction temperature (K). Kinetic parameters for each reaction are listed in Table 1 where ΔH is the heat of reaction (kJ/kg).

Table 1: Kinetic parameters for the Di Blasi biomass pyrolysis scheme.

Reaction	A (1/s)	E (kJ/mol)	ΔH (kJ/kg)	Reference
1	4.38×10^9	152.7	-20	[3]
2	3.27×10^6	111.7	-20	[3]
3	1.08×10^{10}	148.0	255	[3]
4	4.28×10^6	108.0	-42	[2]
5	1.00×10^6	108.0	-42	[2]
6	5.13×10^6	87.6	2700	?

3.4 CFD-DEM simulation

A coarse-grained CFD-DEM model was implemented for biomass pyrolysis in MFiX, an open-source, Fortran-based code [X]. The implemented coarse-grained CFD-DEM model in this research is an extension of the standard MFiX release. Gas phase transport was described using conservation equations of mass, momentum, energy, and chemical species in the Eulerian framework (Equations 14–17, respectively).

$$\frac{d(\epsilon_g \rho_g)}{dt} + \nabla(\epsilon_g \rho_g u_g) = S_\rho \tag{14}$$

$$\frac{d(\epsilon_g \rho_g u_g)}{dt} + \nabla(\epsilon_g \rho_g u_g u_g) = -\epsilon_g \nabla p + \nabla(\epsilon_g \tau) + \epsilon_g \rho_g g + S_u \tag{15}$$

$$\frac{d(\epsilon_g \rho_g E)}{dt} + \nabla(\epsilon_g \rho_g u_g E) = -\nabla Q + S_E \tag{16}$$

$$\frac{d(\epsilon_g \rho_g Y_i)}{dt} + \nabla(\epsilon_g \rho_g u_g Y_i) = -\nabla(D_i \nabla Y_i) + S_{Y_i} \tag{17}$$

where ϵ_g, ρ_g, u_g, p, τ, Q, and Y_i are gas phase volume fraction, density, velocity, pressure, stress tensor, conductive heat flux, and ith chemical species, respectively, t is time, g is acceleration due to gravity, D_i is mass diffusion coefficient for species, S_ρ, S_u, S_E, and S_{Y_i} are mass, momentum, energy, and chemical species source terms, respectively. Fixed quantities of discrete particles with identical initial conditions were lumped into a computational coarse-grained parcel (CGP), whose motion was governed by Newton's second law of motion. All particle forces and contact dynamics were calculated on the parcel scale, whereas heat and mass transfers were calculated on particle scale and projected to the entire parcel. Accordingly, all particles in same coarse- grained parcel possess identical temperature, chemical species concentration, and momentum. The mass and diameter of each coarse-grained parcel was such that:

$$m_{CGP} = m_p W \tag{18}$$

$$d_{CGP} = d_p W^{1/3} \tag{19}$$

where m_{CGP} is CGP mass, m_p is distinct particle mass, W parcel statistical weight, d_{CGP} is CGP diameter, and d_p is distinct particle diameter. Instantaneous accelerations (translational and rotational) for each coarse-grained parcel were calculated as:

$$\frac{du_{CGP}}{dt} = g - \frac{F_p}{m_{CGP}} + \frac{F_c}{m_{CGP}} + \frac{F_d}{m_{CGP}} \tag{20}$$

$$\frac{d\omega_{CGP}}{dt} = \frac{T_{CGP}}{I_{CGP}} \tag{21}$$

where u_{CGP} and ω_{CGP} are the CGP translational and rotational velocities, g is acceleration due to gravity, m_{CGP} is CGP mass, T_{CGP} is net torque on the CGP, and I_{CGP} is CGP moment of inertia. The term F_p represents pressure gradient force and is calculated as product of the CGP volume and pressure gradient. The CGP collision forces F_C (parcel-parcel and parcel-wall collisions) was modeled according linear spring-dashpot model [18]. Since the number of CGP collisions is significantly lower than the number of collisions expected in system with distinct particles, the CGP coefficient of restitution was modified as a correction for energy dissipations during collisions. The proposed modification to the CGP coefficient of restitution is calculated following kinetic theory of granular flow [13] as:

$$e_{CGP} = \sqrt{1 + (e_p^2 - 1)W^{1/3}} \tag{22}$$

where e_{CGP} is CGP coefficient of restitution and e_p is distinct particle coefficient of restitution. Two different drag models were used to estimate CGP drag force F_d based on well-documented difference in the fluidization behavior of sand and biomass in the literature [19]. Drag force was estimated following Ganser-corrected Gidaspow drag model for sand (bed material) particles and a filtered drag model for biomass particles. Th Ganser correction [6] was coupled to the Gidaspow model [8] to account for non-sphericity of the sand particles as expressed below:

$$\beta_{Ganser} = \begin{cases} \beta_{Ergun} & \text{if } \epsilon_g \leq 0.8 \\ \beta_{WenYu} & \text{if } \epsilon_g > 0.8 \end{cases} \tag{23}$$

$$\beta_{Ergun} = 150\frac{(1-\epsilon_g)^2\mu_g}{\epsilon_g d_{CGP}^2\phi^2} + 1.75\frac{(1-\epsilon_g)\rho_g}{\epsilon_g d_{CGP}\phi}|u_g - u_{CGP}| \tag{24}$$

$$\beta_{WenYu} = \frac{3}{4}C_d\frac{(1-\epsilon_g)\rho_g}{d_{CGP}\phi}|u_g - u_{CGP}|\epsilon_g^{-2.65} \tag{25}$$

$$C_d = \begin{cases} \frac{24}{ReK_1}(1 + 0.1118(ReK_1K_2)^{0.6567}) + \frac{0.4305K_2}{1+\frac{3305}{ReK_1K_2}} & \text{if } Re < 1,000 \\ 0.44 & \text{if } Re \geq 1,000 \\ 0.0 & \text{if } Re = 0.0 \end{cases} \tag{26}$$

$$K_1 = \left(\frac{1}{3} + \frac{2}{3}\phi^{-0.5}\right)^{-1} - 2.25\frac{d_{CGP}}{D} \tag{27}$$

$$K_2 = 10^{1.8148(-log\phi)^{0.5743}} \tag{28}$$

The filtered drag model (modified Sarkar drag model) used in this research for biomass particles was proposed by Gao et al. [7] and was found by the authors to have relatively high prediction strength across multiple flow regimes in fluidized bed. The modified Sarkar drag model is derived fine-grid simulation with Wen-Yu drag model and can be computed as:

$$\beta_{Sarkar} = \beta_{WenYu}(1 - H_{Sakar}) \tag{29}$$

$$H_{Sakar} = \begin{cases} 0.95\left(1 - e^{-\alpha_1\alpha_2(u^*_{\text{slip}} - u_0)^p}\right) & u^*_{\text{slip}} > u_0 \\ 0.0 & u^*_{\text{slip}} \leq u_0 \end{cases} \tag{30}$$

$$u^*_{\text{slip}} = \frac{|u_g - u_{CGP}|}{u_t} \tag{31}$$

$$\alpha_1 = \frac{\left(a_1 + a_2(1-\epsilon_g) + a_3(1-\epsilon_g)^2 + a_4(1-\epsilon_g)^3 + a_5(1-\epsilon_g)^4\right)}{1 + e^{100((1-\epsilon_g)-0.55)}} \tag{32}$$

$$\alpha_2 = \left(1 + \frac{a_6}{\Delta^*_{\text{filter}}} + \frac{a_7}{(\Delta^*_{\text{filter}})^2}\right)\left(1 + \frac{a_8}{(u^*_{\text{slip}})^2}\right) \tag{33}$$

$$u_0 = \frac{a_9 + a_{10}(1-\epsilon_g)}{0.01 + (1-\epsilon_g)^{a_{11}}}\left(1 + \frac{a_{12}}{\Delta^*_{\text{filter}}} + \frac{a_{13}}{(\Delta^*_{\text{filter}})^2}\right) \tag{34}$$

$$p = \left(a_{14} + a_{15}(1-\epsilon_g) + a_{16}(1-\epsilon_g)^2\right)\left(1 + \frac{a_{17}}{\Delta^*_{\text{filter}}} + \frac{a_{18}}{(\Delta^*_{\text{filter}})^2}\right) \tag{35}$$

$$\Delta^*_{\text{filter}} = max\left(\frac{g\Delta_{\text{filter}}}{u_t^2},\ \frac{1}{2}\right) \tag{36}$$

$$\Delta_{\text{filter}} = 2(\Delta_x \times \Delta_y \times \Delta_z)^{1/3} \tag{37}$$

$$u_t = \frac{g d^2_{CGP}(\rho_{CGP} - \rho_g)}{18\mu_g} \tag{38}$$

$$\begin{matrix} a_1 & a_2 & a_3 \\ a_4 & a_5 & a_6 \\ a_7 & a_8 & a_9 \\ a_{10} & a_{11} & a_{12} \\ a_{13} & a_{14} & a_{15} \\ a_{16} & a_{17} & a_{18} \end{matrix} = \begin{matrix} 0.75597773 & 2.73931487 & -5.60196497 \\ -1.65853820 & 16.70299223 & -0.44145335 \\ 0.18195034 & -0.01827347 & 0.28441799 \\ -1.943573770 & 0.22177961 & 0.31175890 \\ -0.15971960 & 0.47750002 & 0.062794180 \\ 5.13011673 & 0.67680355 & -0.54535726 \end{matrix} \tag{39}$$

4 Model parameters

Parameters for the reduced-order model and CFD simulations are provided in Tables 2 and 3. Biomass particle characteristics and properties are representative of loblolly pine. Bed particle characteristics are for typical sand material. Operating conditions and reactor dimensions are based on the previously discussed NREL 2FBR fluidized bed pyrolysis unit.

Table 2: Particle parameters for the biomass and bed material (sand). Diameters represent the Sauter-mean diameter.

Parameter	Value	Units	Description
$d_{p\,bed}$	235	μm	bed particle diameter
ϕ_{bed}	0.86	–	bed particle sphericity
ρ_{bed}	2,500	kg/m^3	bed particle density
$d_{p\,bio}$	135	μm	biomass particle diameter
ϕ_{bio}	0.0	–	biomass particle sphericity
ρ_{bio}	540	kg/m^3	biomass particle density

Table 3: Reactor parameters for the bubbling fluidized bed pyrolysis reactor.

Parameter	Value	Units	Description
d_{inner}	5.25	cm	inner reactor diameter
$H_{reactor}$	43.18	cm	reactor height
H_{static}	10.16	cm	static bed height
P_{gas}	101.325	kPa	gas pressure
T_{gas}	773.15	K	gas temperature
Q_{gas}	14	SLM	inlet gas flowrate

Table 4 represents the CFD simulations conducted for this paper. Each row is for a different simulation case which is performed for a particular gas composition.

Table 4: Simulation cases for different gas mixtures where columns denote gas percentage.

Case	N_2	H_2	H_2O	CO	CO_2	CH_4
1	100	0	0	0	0	0
2	0	100	0	0	0	0
3	0	0	100	0	0	0
4	0	0	0	100	0	0
5	0	0	0	0	100	0
6	0	0	0	0	0	100
7	20	20	0	20	20	20
8	50	0	0	0	50	0
9	50	0	0	50	0	0
10	0	0	50	50	0	0
11	100	0	0	0	0	0
12	80	20	0	0	0	0
13	60	40	0	0	0	0
14	50	50	0	0	0	0
15	40	60	0	0	0	0
16	30	70	0	0	0	0
17	20	80	0	0	0	0
18	15	85	0	0	0	0
19	10	90	0	0	0	0
20	5	95	0	0	0	0
21	0	100	0	0	0	0

Table 5: Particle properties for biomass and bed material (sand).

Parameter	Biomass	Sand	Units	Description
d_p	see Table X	453	μm	particle diameter
ρ_p	see Table X	2,500	kg/m^3	particle density
C_p	*	830	kJ/(kg K)	particle heat capacity
ϕ	–	0.94	–	particle sphericity
e_p	0.2	0.61	–	particle-particle coefficient of restitution
e_w	0.2	0.61	–	particle-wall coefficient of restitution
e_s	0.2	–	–	particle-sand coefficient of restitution
μ_p	0.1	0.1	–	particle-particle coefficient of friction
μ_w	0.2	0.2	–	particle-wall coefficient of friction
μ_s	0.1	–	–	particle-sand coefficient of friction
k_n	100	100	N/m	sand particle spring constant

Table 6: Particle size distribution of biomass feedstock.

Sauter mean diameter (μm)	Mass fraction (%)	Mass flow rate (kg/hr)
278	12.1	0.018
344	51.0	0.076
426	34.2	0.051
543	2.7	0.004

Table 7: Chemical species composition of biomass feedstock.

Species	Mass fraction (%)	Density (kg/m^3)
moisture	4.0	1,000
wood	95.9	500
ash	0.1	2,000
char	0.0	300

Table 8: Simulation parameters settings.

Parameter	Value
CFD cell size, $\Delta_x \times \Delta_y \times \Delta_z$ (mm)	$4.2857 \times 4.4 \times 4.3750$
time step, Δ_x (s)	varies
biomass parcel statistical weight	10
sand parcel statistical weight	20
gas phase equation of state	ideal

5 Results and discussion

This section provides results and related discussions for the effects of different fluidization gases on the operation and conversion of a bubbling fluidized bed reactor.

5.1 Comparison of gas properties

Molecular weight, viscosity, density, thermal conductivity, heat capacity, and Prandtl number of the individual gases investigated in this paper are shown in Figure 5. The gas properties were calculated at a pressure of 101,325 Pa and a temperature of 773.15 K (500°C). The lightest gas in terms of molecular weight and density is hydrogen while the heaviest gas is carbon dioxide. The highest viscosity is noted for the nitrogen gas while hydrogen has the lowest viscosity. The largest thermal conductivity is for hydrogen at approximately 0.36 W/(m K) while the other gases remain below 0.12 W/(m K). The highest

heat capacity is obtained for methane at 62 J/(mol K) while the lowest is for hydrogen at 29 J/(mol K). The Prandtl number is similar for all the gases except for water vapor.

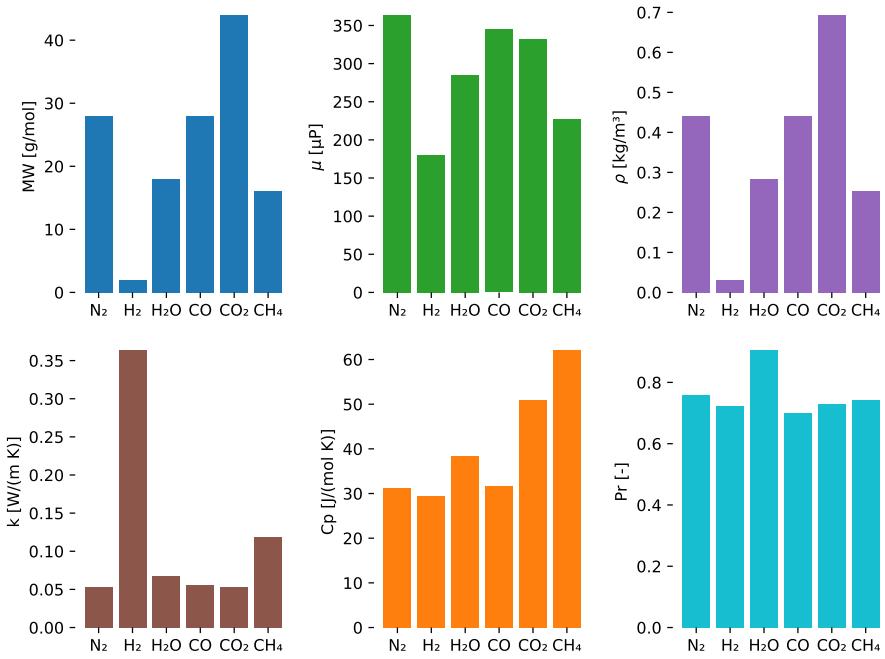

Figure 5: Comparison of molecular weight (MW), viscosity (μ), density (ρ), thermal conductivity (k), heat capacity (Cp), and Prandtl number (Pr) for each gas at 101,325 Pa and 773.15 K (500°C).

Properties for molecular weight, viscosity, and density for the gas mixtures investigated in this paper are shown in Figure 6. Similar to the individual gas properties, the mixture properties were calculated at 101,325 Pa and 773.15 K (500°C). The fraction of each gas in the mixture is given by the values shown at the top of each column in the figure. For example, the hydrogen and nitrogen mixture is comprised of 80% hydrogen and 20% nitrogen which is labeled as $0.8 + 0.2$. As expected, the carbon dioxide mixture is the heaviest in terms of molecular weight and density.

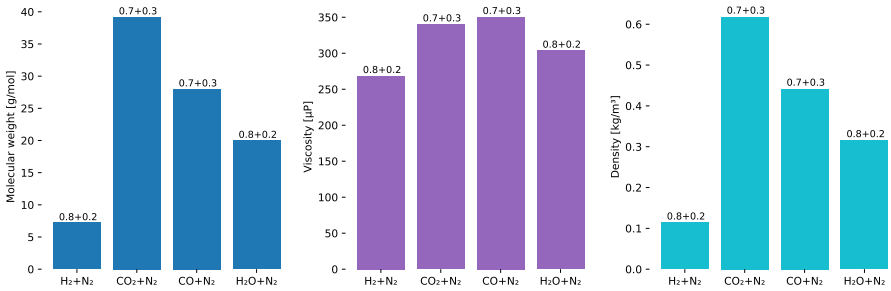

Figure 6: Comparison of gas mixture properties for molecular weight, viscosity, and density at 101,325 Pa and 773.15 K. Fraction of each gas component is shown at the top of each column.

5.2 Fluidization effects

Minimum fluidization velocity (Umf) of the bed material for the different fluidization gases is presented in Figure 7. The hydrogen gas requires about twice the gas velocity to fluidize the sand bed compared to the nitrogen gas.

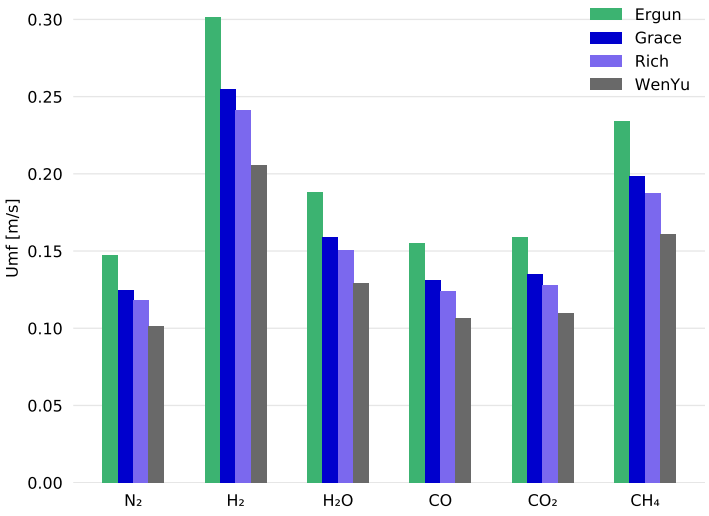

Figure 7: Comparison of minimum fluidization velocity (Umf) for different fluidization gases. Values calculated with the Ergun, Grace, Richardson, and Wen and Yu correlations.

5.3 Evaluation of the kinetic scheme

The Di Blasi kinetics were put to use in a batch reactor model to investigate the time scales associated with the reaction mechanisms. Figure 8 is an overview of the biomass conversion and product yields using the Di Blasi kinetics in a batch reactor at 773.15 K (500°C). At this temperature, without the effects of secondary reactions, the kinetics offer a maximum achievable tar yield of 78% within 5 seconds. However, if secondary reactions occur during the entire pyrolysis process then a maximum tar yield of only 53% is possible. The Di Blasi kinetics suggest that minimizing the extent of secondary reactions is critical to producing the maximum possible tar yield.

A range of reaction temperatures were applied to the Di Blasi kinetics in the batch reactor model as shown in Figure 9. The kinetics suggest that temperature has a neglible effect on primary tar yield but effects of secondary reactions are more pronounced. When secondary reactions occur during the entire pyrolysis process, maximum tar yields are realized at higher temperatures but with shorter residence times. These results suggest that if secondary reactions are minimized then temperature should not have a drastic effect on tar yield.

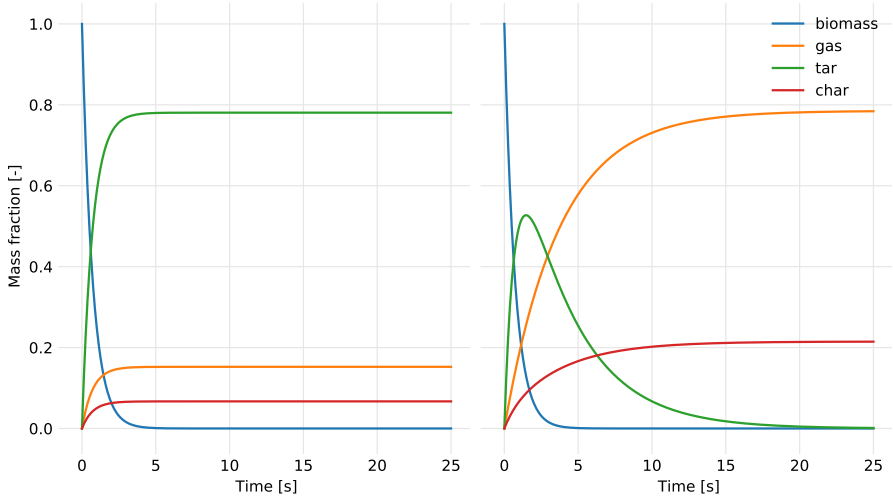

Figure 8: Biomass conversion and product yields in a batch reactor model at 773.15 K (500°C) according to the Di Blasi kinetic reactions. Results shown for primary reactions only (left) along with primary and secondary reactions (right).

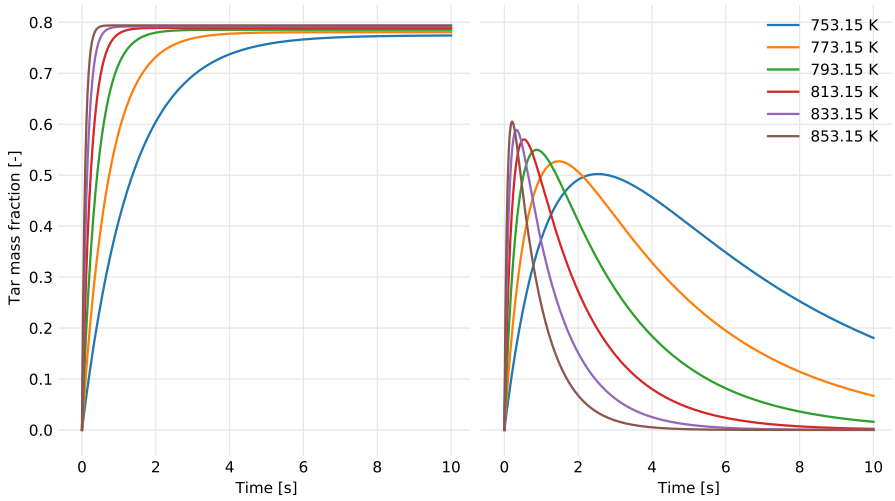

Figure 9: Tar yields for reaction temperatures of 753.15–853.15 K (480–580°C) using the Di Blasi kinetics in a batch reactor model. Results shown for primary tar (left) along with primary and secondary tar (right).

5.4 Comparison of pyrolysis yields

Here.

6 Conclusion

Here.

7 Source code

Python models used to generate results for this article are available on the CCPC GitHub at `https://github.com/ccpcode` in the X repository. Functionality provided by the Chemics package was used for gas properties and various fluidization calculations. See the Chemics documentation at `https://chemics.github.io` for more information.

References

[1] M. Asadullah et al. “Jute stick pyrolysis for bio-oil production in fluidized bed reactor”. In: *Bioresource Technology* 99 (2008), pp. 44–50.

[2] Colomba Di Blasi. "Analysis of Convection and Secondary Reaction Effects Within Porous Solid Fuels Undergoing Pyrolysis". In: *Combustion Science and Technology* 90 (1993), pp. 315–340.

[3] Colomba Di Blasi and Carmen Branca. "Kinetics of Primary Product Formation from Wood Pyrolysis". In: *Industrial & Engineering Chemistry Research* 40 (2001), pp. 5547–5556.

[4] A.V. Bridgwater. "Principles and practice of biomass fast pyrolysis processes for liquids". In: *Journal of Analytical and Applied Pyrolysis* 51 (1999), pp. 3–22.

[5] Tony Bridgwater. "Challenges and Opportunities in Fast Pyrolysis of Biomass: Part I". In: *Johnson Matthey Technology Review* 62.1 (2018), pp. 118–130.

[6] Gary H. Ganser. "A rational approach to drag prediction of spherical and nonspherical particles". In: *Powder Technology* 77.2 (1993), pp. 143–152. DOI: https://doi.org/10.1016/0032-5910(93)80051-B. URL: http://www.sciencedirect.com/science/article/pii/003259109380051B.

[7] Xi Gao et al. "Development and validation of an enhanced filtered drag model for simulating gas-solid fluidization of Geldart A particles in all flow regimes". In: *Chemical Engineering Science* 184 (2018), pp. 33–51. DOI: https://doi.org/10.1016/j.ces.2018.03.038. URL: http://www.sciencedirect.com/science/article/pii/S0009250918301726.

[8] Dimitri Gidaspow. *Multiphase Flow and Fluidization: Continuum and Kinetic Theory Descriptions*. Academic Press, Inc., 1994.

[9] Thomas Graham. "On the Motion of Gases". In: *Philosophical Transactions of the Royal Society of London* 136 (1846), pp. 573–631.

[10] F. Herning and L. Zipperer. "Calculation of the Viscosity of Technical Gas Mixtures From the Viscosity of the Individual Gases". In: *Gas-und Wasserfac* 79 (1936), pp. 69–73.

[11] Daniel Howe et al. "Field-to-Fuel Performance Testing of Lignocellulosic Feedstocks: An Integrated Study of the Fast Pyrolysis-Hydrotreating Pathway". In: *Energy & Fuels* 29 (2015), pp. 3188–3197.

[12] Daizo Kunii and Octave Levenspiel. *Fluidization Engineering*. 2nd ed. Chemical Engineering. Butterworth-Heinemann, 1991.

[13] Liqiang Lu et al. "EMMS-based discrete particle method (EMMS–DPM) for simulation of gas–solid flows". In: *Chemical Engineering Science* 120 (2014), pp. 67–87. DOI: https://doi.org/10.1016/j.ces.2014.08.004. URL: http://www.sciencedirect.com/science/article/pii/S0009250914004229.

[14] Ofei D. Mante et al. "The influence of recycling non-condensable gases in the fractional catalytic pyrolysis of biomass". In: *Bioresource Technology* 111 (2012), pp. 482–490.

[15] Pelle Mellin, Efthymios Kantarelis, and Weihong Yang. "Computational fluid dynamics modeling of biomass fast pyrolysis in a fluidized bed reactor, using a comprehensive chemistry scheme". In: *Fuel* 117 (2014), pp. 704–715.

[16] Dinesh Mohan, Charles U. Pittman, and Philip H. Steele. "Pyrolysis of Wood/Biomass for Bio-oil: A Critical Review". In: *Energy & Fuels* 20 (2006), pp. 848–889.

[17] Charles A. Mullen, Akwasi A. Boateng, and Neil M. Goldberg. "Production of Deoxygenated Biomass Fast Pyrolysis Oils via Product Gas Recycling". In: *Energy & Fuels* 27.7 (2013), pp. 3867–3874.

[18] Helio A. Navarro and Meire P. de Souza Braun. "Determination of the normal spring stiffness coefficient in the linear spring–dashpot contact model of discrete element method". In: *Powder Technology* 246 (2013), pp. 707–722. DOI: https://doi.org/10.1016/j.powtec.2013.05.049. URL: http://www.sciencedirect.com/science/article/pii/S0032591013004178.

[19] T.J.P. Oliveira, C.R. Cardoso, and C.H. Ataíde. "Bubbling fluidization of biomass and sand binary mixtures: Minimum fluidization velocity and particle segregation". In: *Chemical Engineering and Processing: Process Intensification* 72 (2013), pp. 113–121. DOI: https://doi.org/10.1016/j.cep.2013.06.010. URL: http://www.sciencedirect.com/science/article/pii/S025527011300158X.

[20] K. Papadikis, S. Gu, and A.V. Bridgwater. "Computational modelling of the impact of particle size to the heat transfer coefficient between biomass particles and a fluidised bed". In: *Fuel Processing Technology* 91 (2010), pp. 68–79.

[21] Anna Trendewicz et al. "Evaluating the effect of potassium on cellulose pyrolysis reaction kinetics". In: *Biomass and Bioenergy* 74 (2015), pp. 15–25.

[22] Carl L. Yaws. *Yaws' Critical Property Data for Chemical Engineers and Chemists*. Knovel, 2014.

[23] Huiyan Zhang et al. "Biomass fast pyrolysis in a fluidized bed reactor under N2, CO2, CO, CH4 and H2 atmospheres". In: *Bioresource Technology* 102 (2011), pp. 4258–4264.